

# Towards Scalable and Unified Example-based Explanation and Outlier Detection

Penny Chong, Ngai-Man Cheung, Yuval Elovici, and Alexander Binder

**Abstract**—When neural networks are employed for high-stakes decision making, it is desirable for the neural networks to provide explanation for their prediction in order for us to understand the features that have contributed to the decision. At the same time, it is important to flag potential outliers for in-depth verification by domain experts. In this work we propose to unify two differing aspects of explainability with outlier detection. We argue for a broader adoption of prototype-based student networks capable of providing an example-based explanation for its prediction and at the same time identify regions of similarity between the predicted sample and the examples. The examples are real prototypical cases sampled from the training set via our novel iterative prototype replacement algorithm. Furthermore, we propose to use the prototype similarity scores for identifying outliers. We compare performances in terms of classification, explanation quality, and outlier detection of our proposed network with other baselines. We show that our prototype-based networks beyond similarity kernels deliver meaningful explanation and promising outlier detection results without compromising classification accuracy.

**Index Terms**—prototypes, explainability, LRP, outlier detection, pruning, image classification.

## I. INTRODUCTION

DEEP neural networks (DNNs) are widely used in various fields as they show superior performance. Explainable AI, aiming at transparency for predictions [1]–[3] has gained research attention in the recent years. Since humans are known to generalize fast from a few examples, it is suitable to explain a prediction of a test sample via a set of similar examples. Such example-based explanation can simply be achieved using a similarity search over an available dataset based on a metric defined by the feature maps obtained from the trained model. To achieve this, one natural option is to search in an available dataset for the nearest candidates to the test sample in the feature map space. This yields an informative visualization of the feature embedding learned by the model, yet the similar examples found do not participate in the prediction of the test sample. Even if these similar examples share the same prediction with the test sample and are close in feature space, it is not obvious to what *quantifiable extent* the model shares the same reasoning between examples and the test sample, and which parts of test sample and nearest neighbors share the same features. An alternative to achieve such explanation by examples is to employ kernel-based predictors [4]. These methods compute a weighted sum of similarities between the test and the training samples, and thus the impact of each training sample on the prediction of the test sample is naturally quantifiable. Although neural networks perform very well these days without the need for kernel-based setups, one may consider to train a prototype-based student network from an

arbitrarily structured teacher network to provide an example-based explanation<sup>1</sup>. The prototypes in the student network participate in the network prediction and this resembles the participation of training samples in kernel-based predictions.

In this work we propose to unify two aspects of explanation with outlier detection, independent of the structure of the original model, by employing a prototype-based student network to address the three goals. The explanation for predictions is given by the network in these two aspects: i) the top- $k$  most similar prototypical examples and ii) regions of similarity between the prediction sample and the top- $k$  prototypes. Contrasting previous prototype learning approaches [5]–[11], we refrain from directly training prototype vectors in the latent space to avoid reconstruction errors when visualizing the learned prototype vectors in the input space. In lieu of this, we introduce an auxiliary output branch in the network for iterative prototype replacement along the lines of prototype selection methods [12]–[14] to select representative training examples for prediction as inspired by the dual kernel Support Vector Machines (SVM) [4]. Our method omits the need to map or decode prototype vectors and guarantees an explanation relative to real examples present in the training distribution. The prototype importance weight learned via the prototype replacement auxiliary loss also enables pruning of uninformative prototypes.

With the proposed approach, we have to consider the question of performance tradeoff when converting a standard CNN teacher network into a prototype-based student network. We quantify the performance of the predictors in the following three aspects: prediction accuracy, the quality of explanation of the student network as compared to the teacher network, and finally the competence of each predictor in quantifying the outlierness of a given sample. The first two aspects are the natural tradeoffs to be considered when training any surrogate model, while the last aspect measures the outlier sensitivity of predictors in high-stakes environments. It is necessary for predictors deployed in high-stakes settings to be equipped with the capability to flag inputs which are either anomalous or poorly represented by the training set for additional validation by experts. Prototype-based approaches deliver this property naturally by the sequence of sorted similarities between the test sample and the prototypes even though they are not trained primarily for outlier detection. The following summarizes our contribution in this work:

<sup>1</sup>The teacher network is a typical convolutional neural network (CNN) for image classification task. The soft-labels obtained from the teacher will be used for student-teacher learning to train a prototype-based student network.

- (1) We argue for unified interpretable models capable of explanation and detecting outliers with prototypical examples. We demonstrate that a student network based on prototypes is capable of performing two types of explanation tasks and one outlier task simultaneously. We select prototypes from the training set which guarantee that the explanation based on examples comes from the true data distribution.

The prototype network provides two layers of explanation, firstly by identifying the top- $k$  nearest prototypical examples, and secondly, by showing the pixel evidences of similarity between each of these examples and the test sample. The latter is achieved by backpropagating scores from similarity layers using LRP.

- (2) We introduce a novel iterative prototype replacement algorithm relying on training with masks and a widely reusable auxiliary loss term. We demonstrate that this prototype replacement approach scales to larger datasets such as LSUN and PCam.
- (3) We propose various generic head architectures which compute prototype-based predictions from a generic CNN feature extractor and evaluate their prediction accuracy, explanation quality, and outlier detection performance.
- (4) We revisit a method to quantify the degree of outlierness for a sample based on the sorted prototype similarity scores. By doing so, we avoid the complex issue of hyperparameter selection in unsupervised outlier detection methods without resorting to problematic tuning on test sets. A smaller contribution lies in the derivation of the prototype similarity scores depending on the network architectures.

## II. RELATED WORK

**Prototype Learning** One of the earliest works in prototype learning is the  $k$ -nearest neighbor ( $k$ -NN) classifier [15]. In the recent years, researchers have proposed to combine DNNs with prototype-based classifiers. The work [5] proposed a framework known as the convolutional prototype learning (CPL), where the prototype vectors are optimized to encourage representations that are intra-class compact and inter-class separable. Subsequently, [6], [7] proposed interpretable prototype networks to provide explanation based on similar prototypes for image and sequence classification tasks, respectively. The former used a decoder, while the latter project each prototype to its closest embedding from the training set. Another work [8] introduced a prototypical part network (ProtoPNet) that is able to present the prototypical cases that are similar to the parts the network looks at. These explanations are used during classification and not created posthoc. HPnet [9] classifies objects using hierarchically organized prototypes that are predefined in a taxonomy and is a generalization of ProtoPNet. Further works in this domain include [10], [11].

Contrasting the aforementioned methods, we select prototypes directly from the training set and do not use trainable prototype vectors. Related works on prototype selection are [12], [13] which involve mining of representative samples such as prototypes and criticism samples to provide an optimally

compact representation of the underlying data distribution. Our work is related to ProtoAttend [14] which selects input-dependent prototypes via an attention mechanism applied between the input and the database of prototype candidates. A notable difference between our work and ProtoAttend is that our prototypes are global prototypes (fixed after network convergence), whereas they learn input-dependent prototypes which require a sufficiently large prototype candidate database and high memory consumption during training to obtain good performance [14]. In terms of explanation, our method is related to [8]–[11]. These methods explicitly focused on a patch-wise representation of prototypes to deliver prototypical part explanation, whereas in our approach, a prototype represents the entire sample and we present a more fine-grained explanation in terms of pixel similarity between the prototype and test sample to explain their respective contribution to the membership of the predicted class using a posthoc explainability method [3].

**Outlier Detection.** We revisit the idea of quantifying outliers using statistics from the set of top- $k$  similarity scores. For this,  $k$ -NN-based distance methods have been frequently considered in the form of summed distances [16], local outlier factors [17], [18], combination of distance and density estimate [19], or kernel-based statistics [20] and such methods are still of recent interest [21] due to favorable theoretical properties. Unlike these works, we are interested in the performance of similarities which do not define a kernel, but rather emerged due to attention-based operations on feature maps. A simple baseline for out-of-distribution detection is the maximum softmax probability method [22] which assumes that erroneously classified samples or outliers exhibit lower probability scores for the predicted class as compared to the correctly classified example. Several other works related to the detection of out-of-distribution samples are [23]–[25]. For comparison, we employ the baseline method [22] for the other predictors and isolation forest [26] to evaluate the effectiveness of the prototype similarity scores derived from our student architectures. Our formulation of the outlier score using the sum of prototype similarity scores is based on the idea in [20] and is also the generalization of the confidence score in ProtoAttend [14].

## III. METHODOLOGY

We employ a student-teacher learning for our proposed prototype-based network to transfer the knowledge from a standard teacher CNN to a prototype-based student network. In this section, we first introduce our prototype network architectures, the iterative prototype replacement algorithm, and the learning objectives. We also present the explainability methods for the network and the formulation of the outlier score with respect to the student architectures.

Our proposed architecture for the student network is inspired by the dual formulation of SVMs [4] that solves the optimization problem  $\max_{\alpha_i \geq 0} \sum_i \alpha_i - \frac{1}{2} \sum_j \sum_k \alpha_j \alpha_k y_j y_k K(\mathbf{x}_j, \mathbf{x}_k)$ , subject to the constraints  $0 \leq \alpha_i \leq C$ ,  $\forall i$  and  $\sum_i \alpha_i y_i = 0$ . For a binary problem, the dual classifier takes the form of  $f(\mathbf{x}) = \sum_i \alpha_i y_i K(\mathbf{x}_i, \mathbf{x}) + b$ , where  $K(\mathbf{x}_i, \mathbf{x})$  is a positive

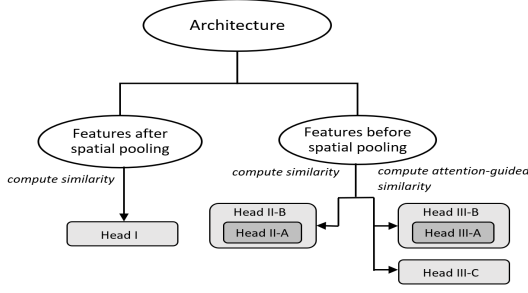


Fig. 1. Taxonomy of the different categories of head architectures proposed for the student network.

definite kernel. The solution is based on the set of similarities  $\{K(\mathbf{x}_i, \mathbf{x}) \mid 1 \leq i \leq N\}$  between the training samples and the test sample  $\mathbf{x}$  which can be used to compute statistics to quantify outliers [20]. We employ here architectures based on attention-weighted similarities beyond Mercer-Kernels.

### A. Proposed Architecture for the Student Network

For the purpose of providing meaningful explanation and detecting outliers, we introduce three generic head architectures<sup>2</sup> for our prototype student network. Each architecture is evaluated for its performance in providing explanation and detecting outliers in Section V. For simplicity, we assume in this section that the prototypical examples are already selected based on our iterative prototype replacement algorithm. We will introduce the algorithm in Section III-B later.

Let  $f(\cdot; \theta_1) : \mathbb{R}^{C_0 \times H_0 \times W_0} \rightarrow \mathbb{R}^{C \times H \times W}$  be the CNN feature extractor before the spatial pooling layer with the learnable parameters  $\theta_1$ . Let  $e(\cdot; \theta_2) : \mathbb{R}^{C \times H \times W} \rightarrow \mathbb{R}^{\tilde{C}}$  be the prototype network with the learnable parameters  $\theta_2$  and  $\tilde{C}$  is the number of classes in the classification task. The overall student network is represented by  $e \circ f$ . For simplicity, we omit the parameters  $\theta_1, \theta_2$  and denote the feature map representation of the input sample  $x$  as  $f(x)$  in this section. We explore various head architectures for the prototype-based student network to determine their suitability for explanation and identifying outliers. We categorize the head architectures for the prototype network into three classes: similarity after spatial pooling, similarity before spatial pooling, and attention-guided similarity before spatial pooling. Figure 1 shows the taxonomy of the various head architectures for the student network and Figures 2-4 are visualization of the head architectures. Our task differs from standard image retrieval task as our task uses prototypes from the training set that participate in the prediction and thus share quantifiable prediction reasoning as the test sample, whereas image retrieval task involves an exhaustive nearest neighbor search over the entire database which does not participate in the prediction and thus does not guarantee similar prediction reasoning between the test sample and its nearest neighbor. Our proposed head architectures do not require any modification to the CNN encoder as compared

to [14] which requires additional linear layers for queries and keys, adding to the overhead during training.

**Head I** architecture is based on a spatial average pooling of the feature maps  $f(\cdot)$ , resulting in a vector  $g(\cdot)$  that consists of only  $C$  feature channels. This is followed by a cosine similarity over the feature channels  $g(\cdot)$ , as seen in Figure 2:

$$s^{(I)}(p_k) = \frac{g(x)^\top g(p_k)}{\|g(x)\| \|g(p_k)\|}. \quad (1)$$

The similarity output  $s^{(I)}(p_k)$  falls in the range of  $[-1, 1]$ . The linear classification layer  $h(x, \{p_1, p_2, \dots, p_K\}) = \sum_{k=1}^K w_k \text{ReLU}(s^{(I)}(p_k)) + b$  then predicts the output logit  $y$ . For this head architecture, the learnable prototype network parameters  $\theta_2$  denote the parameters of the linear layer  $h(\cdot)$ . The linear layer  $h(\cdot)$  in Head I is consistent with the formulation of dual kernel SVM. The linear layers  $h(\cdot)$  in Head II and III as shown in Figures 3 and 4 will have similar dependency on a set of prototypes  $\{p_1, p_2, \dots, p_K\}$ , but they no longer correspond to kernels.

**Head II** architecture in Figure 3, uses the features before spatial pooling to compute similarity scores. Therefore, the similarity layer computes  $s^{(II)}(p_k) \in \mathbb{R}^{H \times W}$ , i.e. one similarity score for each spatial position  $(h, w)$ . We explore two types of similarity function for this head architecture: A) similarity between the input and prototype at the same spatial position  $(h, w)$ , and B) the maximum similarity between input and prototype at a given *input spatial location*  $(h, w)$ . We refer to the former as Head II-A and the latter as Head II-B. The similarity operation for Head II-A (Eq.(2)) and Head II-B (Eq.(3)) at the spatial location  $(h, w)$  is defined as:

$$s_{h,w}^{(II-A)}(p_k) = \sum_c \hat{f}_{c,h,w}(x) \cdot \hat{f}_{c,h,w}(p_k), \quad (2)$$

$$s_{h,w}^{(II-B)}(p_k) = \max_{h',w'} \sum_c \hat{f}_{c,h,w}(x) \cdot \hat{f}_{c,h',w'}(p_k), \quad (3)$$

$$\hat{f}_{c,h,w}(\cdot) = \frac{f_{c,h,w}(\cdot)}{\|f_{\cdot,h,w}(\cdot)\|_2} = \frac{f_{c,h,w}(\cdot)}{\sqrt{\sum_c [f_{c,h,w}(\cdot)]^2}}, \quad (4)$$

where  $f_{c,h,w}(x)$  and  $f_{c,h,w}(p_k)$  are the  $c$ -th features at the spatial location  $(h, w)$  from the feature maps  $f(x)$  and  $f(p_k)$ , respectively. Eq. (3) ensures that the similarity at the spatial location  $(h, w)$  is computed only between the location  $(h, w)$  in  $x$  and the most relevant location  $(h', w')$  in  $p_k$ , i.e. the pair that gives locally the highest cosine similarity score. Its similarity operation is spatially invariant as it considers all spatial location of the prototype  $p_k$  in identifying the most similar feature to the input  $x$ . Head II-A (Eq. (2)) can be viewed as a special case of Head II-B (Eq. (3)). The operation of Head II-B reduces to Head II-A when the maximum similarity between input and prototype for a given *input spatial location*  $(h, w)$ , also occurs at the prototype location  $(h, w)$ . Thus, the Head II-B architecture is considered as the general case of Head II-A. For this category of architectures, the learnable prototype network parameters  $\theta_2$  denote the parameters of the linear layer  $h(\cdot)$ . Note that Head II-B as a maximum over inner products does not define a kernel anymore, as the maximum of two positive definite matrices is not guaranteed to be positive definite. Thus, we employ a non-kernel-based similarity.

<sup>2</sup>The term head architecture refers to the architecture used in the prototype network which is the portion of the network located after the CNN encoder. Figures 2-4 illustrate this.

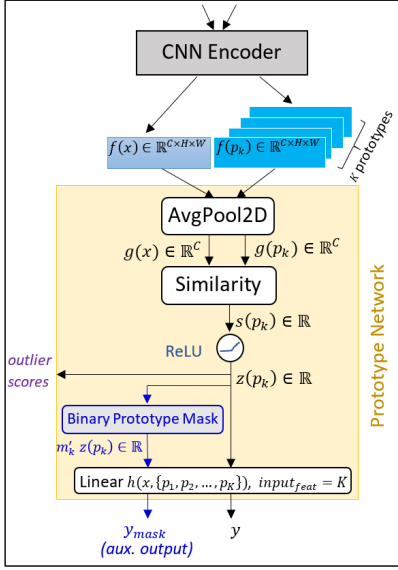


Fig. 2. Head I : Similarity using features after spatial pooling. The  $y_{mask}$  output branch is the auxiliary output branch for iterative prototype replacement.

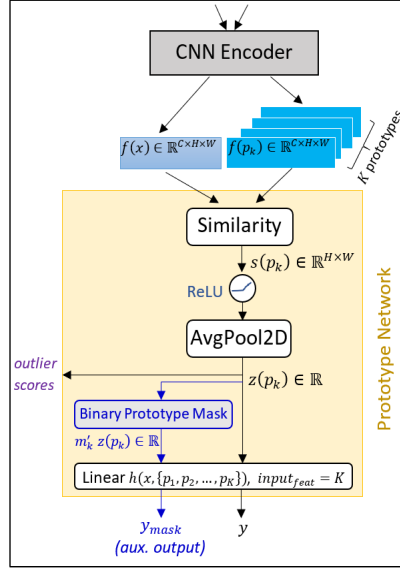


Fig. 3. Head II : Similarity using features before spatial pooling. The  $y_{mask}$  output branch is the auxiliary output branch for iterative prototype replacement.

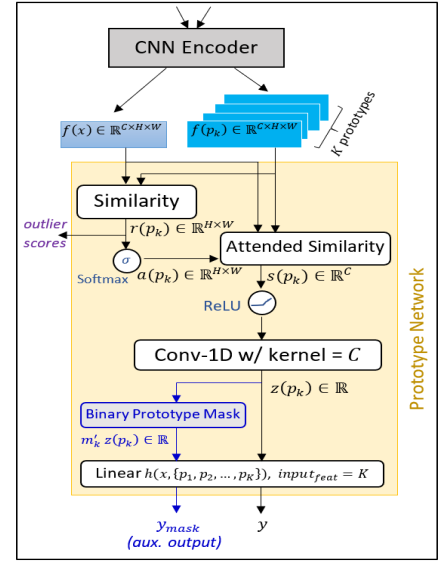


Fig. 4. Head III : Similarity w/attention using features before spatial pooling. The  $y_{mask}$  output branch is the auxiliary output branch for iterative prototype replacement.

#### Algorithm 1 Iterative Prototype Replacement Algorithm

- 1: **Initialization:** Let  $S = D \cup P$  be the original train set with  $n(S) = n(D) + n(P) = N + K$ .  $D$  is the new training set and  $P = \{p_1, \dots, p_k, \dots, p_K\}$  is the set of all prototypes. The initial set  $P$  consists of equal number of samples per class that are randomly sampled from the original train set  $S$ . Let  $\theta_1$  and  $\theta_2$  be the parameters of the CNN feature extractor and the prototype network, respectively, and  $\mathcal{M} \in \mathbb{R}^K$  be the prototype importance weight used for replacement.
- 2: **while**  $e \leq \text{number of epochs}$  **do**
- 3:   **while**  $t \leq \text{number of iterations}$  **do**
- 4:     Perform a forward pass to obtain input features  $f(x)$ , set of prototype features  $\{f(p_k)\}$ , corresponding input features  $\{z(p_k)\}$  of the linear classification layer  $h(\cdot)$ , and the output logits  $y$ . (For Head I, we compute  $g(x)$  and  $\{g(p_k)\}$  instead of  $f(x)$  and  $\{f(p_k)\}$ .)
- 5:     Compute threshold  $\tau_t$  as the  $p$ -th smallest weight in  $\mathcal{M}$ .
- 6:     Compute binary prototype mask  $\mathcal{M}'(\tau_t)$  from  $\mathcal{M}$  as shown in Eq. (11).
- 7:     Perform a forward pass in  $h(\cdot)$  using the masked input to obtain the auxiliary output  $y_{mask}$  as shown in Eq. (12).
- 8:     Optimize parameters  $\theta_1, \theta_2$  and  $\mathcal{M}$  based on the loss function (13).
- 9:   **end while**
- 10:    $P \leftarrow P \setminus P_{replace} \cup D_{rand}$ , where  $P_{replace}$  is the set of  $p$  prototypes with the smallest weight in  $\mathcal{M}$ , and  $D_{rand}$  is the set of random samples comprising of the replaced prototype classes sampled from  $D$  to replace  $P_{replace}$ .
- 11:    $D \leftarrow D \setminus D_{rand} \cup P_{replace}$
- 12:   Reinitialize only the weights in  $\mathcal{M}$  where prototypes are replaced.
- 13: **end while**

**Head III** architecture employs a common attention mechanism to compute weighted similarities. For the Head III architecture as shown in Figure 4, the similarity scores from Eq. (2) and (3) are passed into a softmax  $\sigma(\cdot)$  to obtain the following attention maps:

$$a_{h,w}^{(III-A)}(p_k) = \sigma(s_{h,w}^{(II-A)}(p_k)), \quad (5)$$

$$a_{h,w}^{(III-B)}(p_k) = \sigma(s_{h,w}^{(II-B)}(p_k)). \quad (6)$$

terparts of Head II-A and Head II-B, respectively:

$$s_c^{(III-A)}(p_k) = \sum_{h,w} a_{h,w}^{(III-A)}(p_k) \cdot f_{c,h,w}(x) \cdot f_{c,h,w}(p_k), \quad (7)$$

$$s_c^{(III-B)}(p_k) = \sum_{h,w} a_{h,w}^{(III-B)}(p_k) \cdot f_{c,h,w}(x) \cdot f_{c,h_{\max},w_{\max}}(p_k). \quad (8)$$

The indexes  $h_{\max}$  and  $w_{\max}$  in Eq. (8) are the selected  $h'$  and  $w'$  indexes used in the computation of  $s_{h,w}^{(II-B)}(p_k)$ . The output from the attended similarity layer is passed into a convolutional-1D layer with kernel size  $C$  to compute a

Head III-A and Head III-B are the attention-augmented coun-

weighted sum of the  $C$  features. The convolutional-1D layer has a minimum weight clipping at zero to ensure the outputs are always non-negative in order to apply the explainability method described in Section III-D. Additionally, the use of individual attention maps for the respective features  $f(x)$  and  $f(p_k)$  is also investigated in Head III-C:

$$a_{h,w}^{(\text{III-C})}(p_k) = \sigma \left( \max_{u,v} \sum_c \hat{f}_{c,u,v}(x) \cdot \hat{f}_{c,h,w}(p_k) \right), \quad (9)$$

$$s_c^{(\text{III-C})}(p_k) = \sum_{h,w} a_{h,w}^{(\text{III-B})}(p_k) \cdot f_{c,h,w}(x) \cdot a_{h,w}^{(\text{III-C})}(p_k) \cdot f_{c,h,w}(p_k), \quad (10)$$

where  $a_{h,w}^{(\text{III-B})}$  is the attention score from Eq. (6) for  $f(x)$  at the *input spatial location*  $(h,w)$ , whereas  $a_{h,w}^{(\text{III-C})}$  is the attention score for  $f(p_k)$  at the *prototype spatial location*  $(h,w)$ , as can be seen by the computation of  $\max_{u,v}(\cdot)$  over the spatial locations of  $\hat{f}(x)$ . For the head architectures in this category, the learnable prototype network parameters  $\theta_2$  are the parameters of the convolutional-1D and the linear classification  $h(\cdot)$  layers.

### B. Auxiliary Output Branch for Iterative Prototype Replacement

For the selection of representative prototypes, one can directly learn an importance mask over the entire training set and select those samples with high importance as prototypes. This approach, however, does not scale well to large sample sizes as the number of parameters that must be learned increases proportionally. For approaches such as [14], the database of prototype candidates used must be sufficiently large for successful training as reported in their paper. Instead of learning an importance mask over the entire training set or a large candidate database, we propose to learn a smaller importance mask over a fixed number of  $K$  prototypes. We note that  $K$  is very much smaller than the size of the candidate database [14] used during training or inference. Our approach scales well to large sample sizes since the number of parameters to be learned can now be constrained by  $K$  which also correspond to the final number of prototypes used during inference. We introduce an auxiliary output branch to guide the network to learn a prototype replacement scheme that replaces uninformative prototypes (out of the  $K$  prototypes) with new samples based on the importance or contribution of the current prototypes to the decision boundary of the network. Prototypes that are assigned larger importance weights have higher importance and are unlikely to be replaced. On the other hand, prototypes with smaller importance weights are likely to be replaced with other samples from the training set due to their minimal contribution to the decision boundary of the network.

During training, the network learns a prototype importance weight  $\mathcal{M} \in \mathbb{R}^K$  via an auxiliary loss to quantify the importance of the  $K$  prototypes based on their contribution to the prediction. The auxiliary loss imposes a penalty when informative prototypes that influence the decision boundary of the network are removed, i.e. masked out. The network

parameters  $\theta_1, \theta_2$  and the prototype importance weight  $\mathcal{M}$  are jointly optimized. The formulation of the auxiliary loss will be elaborated further in Section III-C.

The full algorithm for the iterative prototype replacement method is presented in Algorithm 1. We compute the binary prototype mask  $\mathcal{M}'(\tau_t)$  from the prototype importance weight  $\mathcal{M}$  using the threshold  $\tau_t$  at iteration  $t$  as:

$$\mathcal{M}'(\tau_t) = \frac{\max(0, \mathcal{M} - \tau_t)}{|\mathcal{M} - \tau_t|} \in \{0, 1\}. \quad (11)$$

We use the continuous ReLU activation with normalization as inspired by the hard shrinkage operation in [27] to avoid issues with the backpropagation of a discontinuous 0-1 step function. For simplicity, we assign  $\tau_t$  as the  $p$ -th smallest weight in  $\mathcal{M}$  to zero out a fixed number of  $p$  prototypes (in the input of the linear classification layer  $h(\cdot)$ ) with the smallest weight in  $\mathcal{M}$ . To compute the auxiliary output  $y_{mask}$ , we multiply the binary prototype mask  $\mathcal{M}'(\tau_t)$  element-wise with the features  $z(p_k) \in \mathbb{R}$  at the input of the final linear classification layer  $h(\cdot)$  corresponding to each prototype as follows:

$$y_{mask} = h(x, \{p_1, p_2, \dots, p_K\}) = \sum_{k=1}^K w_k m'_k z(p_k) + b, \quad (12)$$

where  $m'_k \in \{0, 1\}$  is the weight in  $\mathcal{M}'(\tau_t)$ , and  $w_k \in \mathbb{R}$  and  $b \in \mathbb{R}$  are the parameters of the linear layer  $h(\cdot)$ . At the end of each epoch, we replace the  $p$  prototypes which have the smallest weight in  $\mathcal{M}$  with new samples from the training set  $D$ . The new set of prototypes  $P$  also maintains equal number of samples per class during training.

The prototype importance weight  $\mathcal{M}$  can also be used to prune prototypes and relevant neurons. This will be discussed in Section VI-B.

### C. Learning Objective

We define the set of input training samples with their groundtruth to be  $D = \{(x_i, \tilde{y}_i) \mid 1 \leq i \leq N\}$  and the set of prototypes with their class labels to be  $P = \{(p_k, \tilde{q}_k) \mid 1 \leq k \leq K\}$ . For an input sample  $x$ , we denote the output logits of the teacher network as  $y_T$ , and the logits and auxiliary output of the student network as  $y$  and  $y_{mask}$ , respectively. The predicted class label from the student network for the input sample  $x$  is represented by  $y_{pred} = \arg \max y$ . The following defines the objective function for our student network:

$$\min_{\theta_1, \theta_2, \mathcal{M}} \mathcal{L}(\tilde{y}, \sigma(y)) + \lambda_1 \mathcal{L}(\sigma(y_T), \sigma(y)) + \lambda_2 \mathcal{L}(y_{pred}, \sigma(y_{mask})) + \lambda_3 \mathcal{J}((x, \tilde{y}), (p, \tilde{q})), \quad (13)$$

where  $\mathcal{L}(\cdot)$  is the cross-entropy loss,  $\mathcal{J}(\cdot)$  is a loss term based on the squared  $L_2$ -norm, and  $\sigma(\cdot)$  is the softmax.

The first two terms are the losses commonly employed in the training of a student network. The second term also known as the distillation loss, is the cross-entropy loss with the teacher soft-labels as ground truth to encourage the student network to learn predictions resembling the teacher network.

The third term  $\mathcal{L}(y_{pred}, \sigma(y_{mask}))$  encourages the learning of parameters such that the network class prediction remains unchanged while relying only on a subset of prototypes which

leads to the dichotomization of important and less important prototypes. This allows the replacement of lower ranked prototypes that have lower impact on the prediction accuracy in the prototype replacement step.

The fourth loss term  $\mathcal{J}((x, \tilde{y}), (p, \tilde{q}))$  encourages the feature space of the input sample  $x$  to be close to the set of prototypes from the same class but further away from the other classes. The formulation of this objective term varies slightly between the different head architectures depending on their similarity operation.

For the Head I architecture, the objective term  $\mathcal{J}((x, \tilde{y}), (p, \tilde{q}))$  is defined as:

$$\frac{1}{|D||P|} \sum_{i=1}^{|D|} \sum_{k=1}^{|P|} (\|\hat{g}(x_i) - \hat{g}(p_k)\|_2^2)^\alpha, \quad (14)$$

where  $\alpha = 1$ , if  $\tilde{y}_i = \tilde{q}_k$ , else  $\alpha = -1$ .

For the Head II-A and Head III-A architectures, the objective function  $\mathcal{J}((x, \tilde{y}), (p, \tilde{q}))$  is defined as:

$$\frac{1}{|D||P|} \sum_{i=1}^{|D|} \sum_{k=1}^{|P|} \left[ \frac{1}{HW} \sum_{h,w,c}^{H,W,C} (\hat{f}_{c,h,w}(x_i) - \hat{f}_{c,h,w}(p_k))^2 \right]^\alpha, \quad (15)$$

where  $\alpha = 1$ , if  $\tilde{y}_i = \tilde{q}_k$ , else  $\alpha = -1$ .

The term inside the square bracket is simply the average squared  $L_2$ -norm computed for the channel dimension over all spatial position  $(h, w)$ . Similarly, the objective function  $\mathcal{J}((x, \tilde{y}), (p, \tilde{q}))$  for the Head II-B and Head III-B architectures is defined as:

$$\frac{1}{|D||P|} \sum_{i=1}^{|D|} \sum_{k=1}^{|P|} \left[ \frac{1}{HW} \sum_{h,w,c}^{H,W,C} (\hat{f}_{c,h,w}(x_i) - \hat{f}_{c,h_{\max},w_{\max}}(p_k))^2 \right]^\alpha, \quad (16)$$

where  $\alpha = 1$ , if  $\tilde{y}_i = \tilde{q}_k$ , else  $\alpha = -1$ .

The different formulation for Eq. (15) and Eq. (16) is due to the two different types of similarity operation introduced in the head architectures as discussed in Section III-A. For Head III-C architecture, the objective function  $\mathcal{J}(\cdot)$  is expressed as

$$\mathcal{J}((x, \tilde{y}), (p, \tilde{q})) = \mathcal{J}_x((x, \tilde{y}), (p, \tilde{q})) + \mathcal{J}_p((x, \tilde{y}), (p, \tilde{q})), \quad (17)$$

where the first term is equivalent to Eq. (16) and the second term is defined accordingly based on the  $a_{h,w}^{(III-C)}(p_k)$  operation for  $f(p_k)$  in Head III-C, i.e. use  $\hat{f}_{c,h_{\max},w_{\max}}(x_i)$  instead of  $\hat{f}_{c,h,w}(x_i)$  and vice versa for  $p_k$  in the loss  $\mathcal{J}_p(\cdot)$ .

#### D. Explanation for Top- $k$ Nearest Prototypical Examples

The student network provides prediction explanation in the form of: (1) prediction explanation with top- $k$  nearest prototypical examples and (2) the pixel evidence of similarity between the prediction sample and the prototypical examples. We define a prototype similarity score  $u_k$  that ranges between  $[0, 1]$  to identify the top- $k$  nearest prototypical examples for a given input sample. We elaborate on the formulation of the prototype similarity score  $u_k$  in Section III-E as the scores are also used to formulate the outlier score. In the following paragraph, we recapitulate the explanation method

to compute pixel evidence of similarity between each pair of input-prototype.

To show evidence of similarity between the input sample and the prototypes in the pixel space, we use a posthoc explainability method, the Layer-wise Relevance Propagation (LRP) algorithm [3] to compute a pair of LRP heatmaps for each pair of input-prototype. For a pair of input-prototype, their respective heatmaps comprise of positive and negative relevance scores (also known as evidences) in the pixel space. The relevance scores represent the pixels' contribution to the prediction score. For the 2D-convolutional layers, we used the following LRP- $\alpha\beta$  rule to compute relevance  $R_d^{(l)}$  for the neuron  $d$  at the current layer  $l$ :

$$R_d^{(l)} = \sum_j \left( \alpha \frac{(a_d w_{dj})^+}{\sum_{0,d} (a_d w_{dj})^+} - \beta \frac{(a_d w_{dj})^-}{\sum_{0,d} (a_d w_{dj})^-} \right) R_j^{(l+1)}, \quad (18)$$

where  $\alpha - \beta = 1$ ,  $\alpha > 0$ ,  $\beta \geq 0$ , and  $R_j^{(l+1)}$  is the relevance for the neuron  $j$  at the succeeding layer  $l+1$ . For the other layers, including the similarity layer (Head I and II) and the attended similarity layer (Head III), we use the following LRP- $\epsilon$  rule:

$$R_d^{(l)} = \sum_j \frac{a_d w_{dj}}{\epsilon + \sum_{0,d} a_d w_{dj}} R_j^{(l+1)}. \quad (19)$$

The similarity/attended similarity layer is treated like a linear layer which enables the easy application of the LRP- $\epsilon$  rule in the standard manner without resorting to more complex LRP methods such as BiLRP [28]. For Head III architectures, the relevance scores flow through the attended similarity layer branch only while treating the attention weights from the similarity layer as constants.

From the last linear layer up to the similarity/attended similarity layer  $l$ , we compute the relevance scores  $R_{(\cdot)}^{(l)}(x, p_k)$  for each pair of  $(x, p_k)$ . Using  $R_{(\cdot)}^{(l)}(x, p_k)$  at the similarity/attended similarity layer  $l$ , we compute the LRP heatmap for  $x$  by backpropagating the relevances to the input space of  $x$  through the CNN encoder. The heatmap for  $p_k$  is also computed in a similar manner (for Head II-B and Head III-B architectures with  $\max_{h',w'}(\cdot)$  operation, the relevance scores are accumulated at the relevant  $h'$  and  $w'$  indexes before backpropagating to the input space of  $p_k$ ). We refer to [3] for more information on LRP algorithms.

#### E. Quantifying the Degree of Outlierness of a Sample

Our proposed prototype-based architectures can naturally quantify the degree of outlierness of an input sample based on the sequence of sorted similarities even though they are not trained primarily for outlier detection. We revisit the method in [20] and generalize the confidence score in [14] to compute an outlier score based on the sum of similarity scores. We use the sum of the prototype similarity scores  $u_k$  to compute the outlier score. While we see the main contribution in unifying two aspects of explanation and outlier detection, a smaller contribution lies in the different formulation of the prototype similarity scores  $u_k$  with respect to the student architecture (refer to the output branch for outlier score in Figures 2-4).

For each input sample  $x$ , we define the set of corresponding prototype similarity scores as  $U = \{u_k \mid 1 \leq k \leq K\}$ . For all Head I and Head II architectures, the  $u_k$  score is assigned as  $u_k = z(p_k)$ , where  $z(p_k)$  is the input to the linear layer  $h(\cdot)$  as shown in Figures 2 and 3. For Head III-A and Head III-B architectures, the  $u_k$  score is computed as  $u_k = \frac{1}{HW} \sum_{h=1, w=1}^{H, W} r_{h,w}(p_k)$ . For the Head III-C architecture, the  $u_k$  score is computed as  $u_k = \max_{h,w}(r_{h,w}(p_k))$ . With the placement of ReLU layers in the CNN, the elements of  $U$  lie in the range of  $[0, 1]$ , where a higher value indicates a larger similarity between the input sample  $x$  and the prototype  $p_k$ . From the set  $U$ , top- $k'$  highest scores are selected regardless of the prototype class. For sample  $x$ , the outlier score  $o(x)$  is defined as:

$$o = 1 - \frac{1}{k'} \sum_{k=1}^{k'} u_k. \quad (20)$$

Note that the  $u_k$  are in general no inner products, and thus we cannot compute true metric distances and follow thus the idea in [20]. In this formulation, we assume that the prototype similarity scores  $u_k$  for outliers are smaller than the normal samples. The above formulation is the general case which considers prototypes from all classes in the summation, unlike the formulation of the confidence score in [14] which considers only the set of prototypes from the predicted class. We show only the results using Eq. (20) which gives better performance and omit results using only prototypes from the same predicted class due to lack of space. Larger outlier score  $o$  indicates larger anomaly.

#### IV. EXPERIMENTAL SETTINGS

**Dataset.** We used the LSUN [29] dataset consisting of 10 classes with the image size  $128 \times 128$  pixels and the PCam [30], [31] dataset consisting of 2 classes with image size  $96 \times 96$  pixels. For the LSUN dataset, we subsampled 10,000 samples per class from the given train set and used the 80 : 20 split for train and validation. The given validation set was used as the test set. We refrained from the common usage of CIFAR-10, MNIST, or Fashion MNIST classes, which are known to cluster very easily and offer little potential for aggregating spatial similarities due to low spatial resolutions. These datasets do not provide an accurate performance benchmark which we explain later in Section V-A.

**LRP Perturbation.** We subsampled only 100 samples per class, from our LSUN test set, and 500 samples per class, from our PCam test set. We set  $\alpha = 1.7$ ,  $\beta = 0.7$ , and  $\epsilon = 1e - 3$  for the LRP- $\alpha\beta$  and LRP- $\epsilon$  rules, respectively.

**Outlier Setup.** Three different types of outlier setups were used in our experiments. Setup A consists of the LSUN test set which is labelled as the normal sample set and the test set from Oxford Flowers 102 [32] dataset which is labelled as the outlier sample set. For Setup B, we created a synthetic outlier counterpart for each test sample in our test set (LSUN/PCam) by drawing random *strokes* of thickness  $M$  on the original image [33]. In Setup C, we created an outlier counterpart for each test sample by manipulating the color of the image, via increasing the minimum saturation and value components, and then randomly rotating the hue component. The manipulated

image has abnormal colors. Due to the large number of test samples in the PCam dataset, 1500 samples per class were sampled from the test set for the outlier detection experiments.

**Model and Hyperparameter.** We used a ResNet-50 [34] pretrained on ImageNet as the CNN encoder and the SGD optimizer with momentum 0.9 and weight decay of  $1e - 4$ . The learning rates of  $1e - 3$  and  $1e - 4$  were used in the prototype network and the CNN encoder, respectively. A decaying learning rate with a step size of 10 epochs and  $\gamma = 0.1$  was also adopted. For the learning objectives, we set  $\lambda_1 = \lambda_2 = 1$  and  $\lambda_3 = 0.1$ . For the iterative prototype replacement algorithm, we set  $p = 30\%$  of the number of prototypes (line 5 of Algorithm 1). We used PyTorch [35] for implementation. We compared our methods with the teacher network, ProtoDNN [6], ProtoPNet [8], and the  $\chi^2$ -kernel SVM [36]. To control architectural effects, we used the same ResNet-50 architecture pretrained on ImageNet as the CNN encoder for the aforementioned methods. We followed strictly the hyperparameters used by the authors except for the learning rate of the encoder in ProtoDNN, which we set to a learning rate of  $1e - 5$ . The  $\chi^2$ -kernel SVM used histogram CNN features pretrained on ImageNet. Since kernel SVMs do not scale to large datasets, we used a  $\chi^2$  approximation kernel [36] and the SGD classifier with hinge loss at optimal learning rate and tolerance of  $1e - 4$ . We performed a grid search on the validation set with the hyperparameters  $\{1e - 5, 1e - 4, \dots, 1\}$  to determine the regularization constant in the SGD classifier. We used 10 and 20 prototypes per class in the LSUN and PCam experiments, respectively.

#### V. EXPERIMENTAL RESULTS

##### A. Prediction Performance

We begin the comparison with the predictive aspect of our proposed architectures and the other methods on both datasets. Based on Table 1, it can be observed that the proposed student architectures outperform the teacher network and are better than the other methods on the LSUN dataset. The Head III-B student network which computes an attention map based on the maximum similarity between input and prototype has the best classification performance among the other student networks. The Head III-C student network which computes individual attention maps for the input and the prototype has similar performance as Head III-B but is computationally more expensive to train due to the additional attention map used. It can be observed that ProtoDNN underperforms severely on the LSUN dataset. A manual inspection of the prototypes from ProtoDNN reveals that the prototypes do not resemble any training samples and the autoencoder used for prototype decoding fails to reconstruct the LSUN samples resulting in poor classification performance. This implies that the joint optimization for the layers in ProtoDNN only performs well on simple grayscale datasets such as MNIST and Fashion MNIST [6], but is not generalizable to complex dataset such as LSUN. Our student network does not rely on autoencoders for prototype visualization, since the prototypes are actual training samples selected from the training set. From our own observation with outlier detection on simpler datasets and the



inability of ProtoDNN to generalize on complex dataset such as LSUN, we refrain from using the common and simple datasets such as MNIST and Fashion MNIST in our evaluation to provide a more challenging performance benchmark.

TABLE I  
CLASSIFICATION PERFORMANCE ON LSUN TEST SET.

Model	Acc. (%)
$\chi^2$ SVM [36]	76.8
ProtoDNN [6]	54.2
ProtoPNet [8]	82.5
Teacher ( <i>baseline</i> )	80.1
Student Head I	82.9
Student Head II-A	82.9
Student Head II-B	82.5
Student Head III-A	82.8
Student Head III-B	<b>83.5</b>
Student Head III-C	83.4

TABLE II  
CLASSIFICATION PERFORMANCE ON PCAM TEST SET.

Model	Acc. (%)	AUC
$\chi^2$ SVM [36]	80.2	0.8875
ProtoDNN [6]	76.7	0.8180
ProtoPNet [8]	<b>83.4</b>	0.8822
Teacher ( <i>baseline</i> )	80.5	0.9142
Student Head I	83.3	<b>0.9216</b>
Student Head II-B	82.5	0.9111
Student Head III-B	81.0	0.9205

For the PCam dataset as shown in Table II, we show only one type of head per category. For Head II and III categories, we show only performances of Head II-B and Head III-B architectures as they are the general cases of Head II-A and Head III-A, respectively, and have lower computational complexity than the Head III-C architecture. Based on Table II, ProtoPNet and our student network with Head I architecture demonstrate equally good performance on the PCam dataset. The former achieves the highest test accuracy (only marginally better than Head I) and the latter achieves the best AUC score. The PCam dataset consisting of only 2 classes and similar image statistics has less intra-class variations as compared to the LSUN dataset with its 10 classes. In this case, Head I which computes similarity using spatially pooled features overfits less, thus performs better than more complex architectures like Head II-B and Head III-B. For the remaining experiments using the PCam dataset, we evaluate only Head II-B and Head III-B for the Head II and Head III categories.

We conclude that using prototype-based students results in models that are equally competitive in prediction performance as the teacher network. Using soft-labels from a teacher network keeps the training of prototype networks stable and allows an unconstrained modeling of the original task.

### B. Top- $k$ Nearest Example and Pixel-wise Explanation

We provide explanation using the top- $k$  nearest prototypical examples from different classes and show the pixel evidences of similarity between the prototype and test sample. We first compare the quality of the pixel-wise LRP heatmap explanation generated by the different student architectures with the

teacher network and then show examples of explanation in the two forms (refer Section III-D).

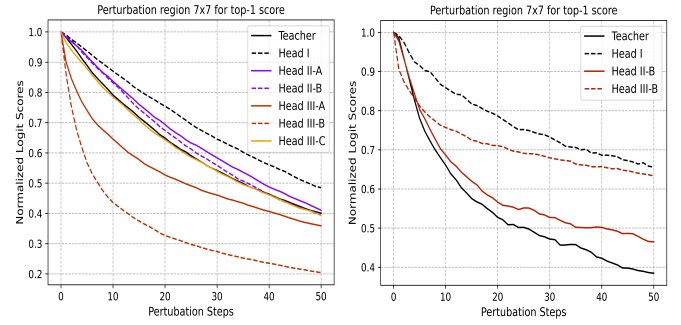


Fig. 5. LRP heatmap quality evaluation on LSUN (left) and PCam (right) datasets. The LRP heatmap perturbation for the student will use the LRP score computed between each test sample and its top-1 prototype.

We assess the quality of the pixel-wise LRP heatmap explanation for the network by performing a series of region perturbations in the input space of the test sample. The LRP heatmap comprises of relevance scores associated with the degree of importance for the predicted class. Performing a perturbation on the image pixel associated with high relevance scores will destroy the network logit for the predicted class. In other words, we expect a sharp decrease in the logit score of the predicted class as the relevant features in the input sample are gradually removed in a decreasing order of importance. We adopt the generalized region perturbation approach in [37]. We perform a series of perturbations starting from the most relevant region (based on the LRP relevance scores) to the least relevant region as shown in Figure 5. A steep decrease in the curve suggests good pixel explanation.

Based on the subplot for LSUN dataset in Figure 5, the Head III-B student architecture with the best classification performance also has the best heatmap explanation as shown by the largest decline in the logit scores. The attention modules in Head III-A and Head III-B show evidently better explanation qualities than the standard teacher network as suggested by their respective curves. The Head I architecture shows poorer explanation than the teacher network due to the early average pooling operation which may have removed distinctive features that are useful in providing an informative pixel explanation. For the PCam dataset, the subplot suggests better heatmap quality for Head III-B architecture in the first 5 perturbation steps only, and is overtaken by the teacher network and the Head II-B student network. Due to a lower diversity of objects in a patch (small cell types, stromal tissue and background) in the PCam dataset as compared to the LSUN dataset, there may be a lesser need for attention weighting for explanation and thus Head II-B shows better LRP explanation than its attention-augmented counterpart Head III-B, when increasing number of relevant regions are perturbed. Likewise, Head I architecture shows poor LRP explanation on the PCam dataset although it achieves the best classification performance in Table II. Generally, architectures with attention mechanism provide better LRP explanation for datasets with large object diversity, while datasets with low object diversity need lesser attention weighting for explanation.



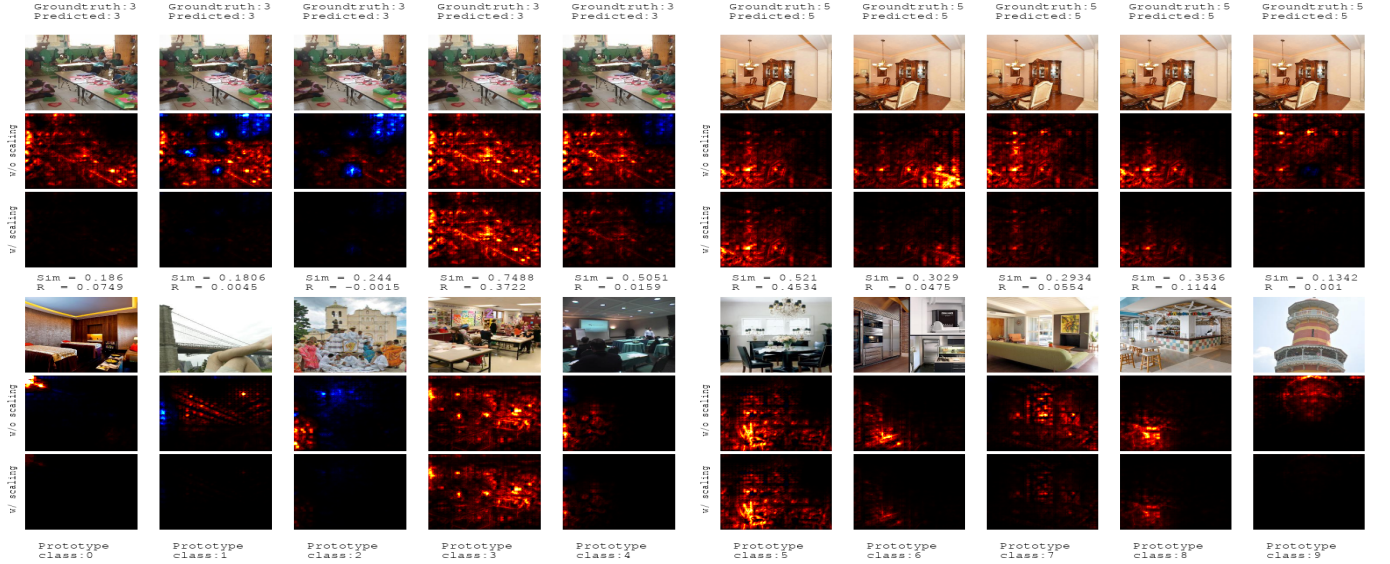


Fig. 6. LRP heatmaps from Head III-B on the LSUN dataset for the prediction *classroom* (left) and *dining room* (right). Subplots in the upper part show heatmaps explaining the input sample, while the lower part show heatmaps explaining the shown prototype. In all subplots, each column corresponds to heatmaps with respect to the top-1 prototype of a specific class. The heatmaps in the second row of the upper and lower parts are unscaled, whereas the heatmaps in the third row are scaled such that the  $(x, p_k)$  pair with lower  $u_k$  score (written as sim score) will appear dimmer.

Due to space constraints, we show only LRP heatmaps from architecture with the best explanation (Head III-B) in Figures 6 and 7. We show pairs of heatmaps between the input sample and the top-1 nearest prototype (based on  $u_k$  score) for a few selected classes. The positive and negative evidences in the heatmaps are represented by red and blue pixels, respectively. We obtain non-identical input heatmaps (the columns in the top half of Figures 6 and 7) when comparing the same input sample with different prototype samples due to the different similarity output computed and thus unequal relevances for each input-prototype pair. In the left part of Figure 6, heatmaps for mostly all classes are dimmed out (the third row in the upper and lower part) after scaling due to their low similarity  $u_k$  scores, except class 3 (*classroom*) which is the predicted class. The red pixels are the similar regions between the pair of input-prototype that has contributed positively to the prediction *classroom*. In the lower right of Figure 6 showing the top-1 prototypes from different classes, the regions that resemble furniture in the dining room such as chairs, tables, and stools generally lit up in the prototype heatmaps for the prediction *dining room*. They mainly correlate to the input regions with dining table, chair, and chandelier) as shown in the upper right of Figure 6. For the explanation on the PCam dataset in Figure 7, we show explanation for a true negative, a true positive, and a false negative. The true negative prediction shows positive relevance scores (in red) on dense clusters of lymphocytes (the dark regular nuclei) which are the evidences supporting the absence of tumor. For the false negative prediction, the input which is a positive sample (as indicated by the groundtruth) resembles more of the negative class prototype (class 0) rather than the positive class prototype (class 1) in the red pixel areas.

Explanation in Figures 6 and 7 allows domain experts to easily validate the reasoning process of the neural networks by verifying that the nearest prototypical training samples

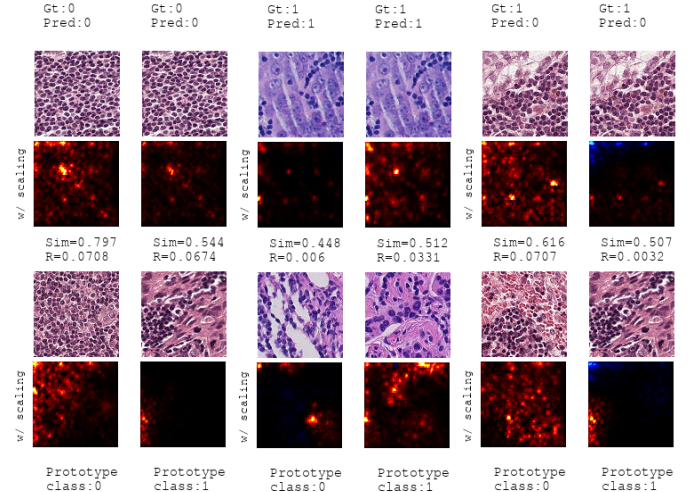


Fig. 7. LRP heatmaps from Head III-B on the PCam dataset. The first two columns are for a true negative (tumor absent), the third and fourth columns are for a true positive (tumor present), and the last two columns are for a false negative.

are correct and the contributing features are relevant to the predicted class. By analyzing contradictory cases of prediction and explanation, domain experts understand the model limitation and is able to make an informed judgement. In summary, Head-II and Head-III architectures show heatmap quality comparable to the teacher network.

### C. Detecting Outliers for Additional Validation

The prototype student networks can naturally quantify the degree of outlieriness using the set of similarity scores. Since we do not optimize the proposed network for outlier detection in the objective function, we do not compare against more sophisticated methods designed primarily to detect outliers but

TABLE III  
OUTLIER DETECTION PERFORMANCE REPORTED USING THE AUC METRIC FOR LSUN NETWORKS.

Model	Setup A Flowers			Setup B LSUN strokes_5			Setup C LSUN altered color		
Isolation Forest [26]	<i>Anomaly Score *</i>			<i>Anomaly Score *</i>			<i>Anomaly Score *</i>		
	0.678			0.687			0.482		
$\chi^2$ SVM [36] ProtoDNN [6] ProtoPNet [8] Teacher ( <i>baseline</i> )	<i>Max Prob.</i> [22]			<i>Max Prob.</i> [22]			<i>Max Prob.</i> [22]		
	0.921			0.742			0.691		
	0.553			0.497			0.520		
	0.847			0.645			0.683		
	0.934			0.677			0.690		
Student Head I	<i>Top-1</i>	<i>Top-20</i>	<i>All proto.</i>	<i>Top-1</i>	<i>Top-20</i>	<i>All proto.</i>	<i>Top-1</i>	<i>Top-20</i>	<i>All proto.</i>
	0.990	<b>0.993</b>	0.739	0.712	0.692	0.473	0.782	<b>0.852</b>	0.630
Student Head II-A	0.970	0.965	0.786	0.764	0.738	0.611	0.809	0.835	0.710
Student Head II-B	0.972	0.984	0.986	0.763	<b>0.765</b>	0.677	0.779	0.790	0.778
Student Head III-A	0.922	0.943	0.885	0.726	0.735	0.683	0.672	0.691	0.636
Student Head III-B	0.855	0.906	0.909	0.692	0.702	0.718	0.674	0.707	0.731
Student Head III-C	0.970	0.972	0.914	0.726	0.727	0.509	0.763	0.786	0.680

\* The anomaly detection algorithm returns an anomaly score for every input sample and such algorithm is not used for classification.

TABLE IV  
OUTLIER DETECTION PERFORMANCE REPORTED USING THE AUC METRIC FOR PCam NETWORKS.

Model	Setup B PCam strokes_5			Setup C PCam altered color		
Isolation Forest [26]	<i>Anomaly Score *</i>			<i>Anomaly Score *</i>		
	<b>0.723</b>			0.580		
$\chi^2$ SVM [36] ProtoDNN [6] ProtoPNet [8] Teacher ( <i>baseline</i> )	<i>Max Prob.</i> [22]			<i>Max Prob.</i> [22]		
	0.521			0.519		
	0.441			0.087		
	0.514			0.450		
	0.527			0.326		
Student Head I	<i>Top-1</i>	<i>Top-20</i>	<i>All proto.</i>	<i>Top-1</i>	<i>Top-20</i>	<i>All proto.</i>
	0.576	0.574	0.511	0.350	0.358	0.820
Student Head II-B	0.678	0.661	0.636	0.377	0.394	<b>0.823</b>
Student Head III-B	0.687	0.631	0.541	0.329	0.249	0.224

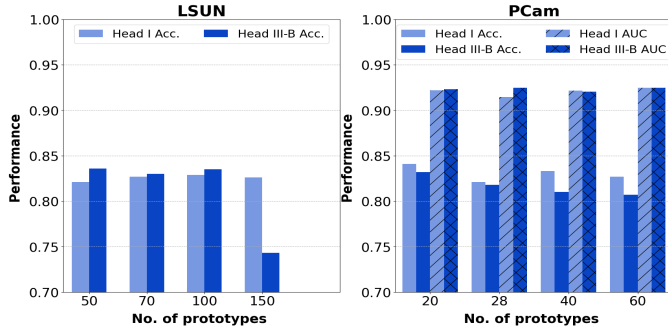


Fig. 8. Impact on performance using different number of prototypes. The x-axis is the total number of prototypes from all classes.

TABLE V  
CLASSIFICATION PERFORMANCE WITHOUT AND WITH PRUNING.

Model	Prune	LSUN	PCam	
		Acc. (%)	Acc. (%)	AUC
Head I	✗	<b>82.9</b>	<b>83.3</b>	<b>0.9216</b>
	✓	82.7	82.6	0.9177
Head II-B	✗	82.5	82.5	0.9111
	✓	<b>82.6</b>	<b>83.3</b>	0.9111
Head III-B	✗	<b>83.5</b>	81.0	0.9205
	✓	83.2	<b>81.8</b>	<b>0.9244</b>

show comparison with the common baseline method based on

the maximum probability class [22] and the classic isolation forest [26] method to evaluate the potential of our prototype networks in distinguishing outliers from the normal sample distribution. The outlier score for the baseline method [22] is the negative probability of the predicted class such that a sample with a smaller predicted class probability has a higher outlier score. The Head I student architecture in Table III achieves the best performance for the flowers and altered color setups using the top-20 prototype similarity scores  $u_k$ . Since the image statistics of the flowers dataset and the altered color anomalies are substantially different from the normal LSUN samples, the use of early spatial pooling before computing similarity in Head I does not remove distinctive features of the anomalies but is effective in detecting outliers, while offering the least potential for overfitting. For the strokes outlier setup, Head II-B has the best detection performance, also using the top-20 prototype similarity scores  $u_k$ . The placement of spatial pooling operation before the similarity operation in Head I may have removed traces of strokes on the image, while Head II-B retains the traces of strokes during the similarity computation. The Head III-B architecture has a higher architectural complexity than Head I and Head II, and is thus less robust to outliers and prone to overfitting. We report detection only on the more challenging setups (strokes and altered color as suggested by the average detection scores

TABLE VI  
OUTLIER DETECTION PERFORMANCE REPORTED USING THE AUC METRIC FOR NETWORKS WITHOUT AND WITH PRUNING.

Model	Prune	LSUN									PCam					
		Setup A Flowers			Setup B LSUN strokes_5			Setup C LSUN altered color			Setup B PCam strokes_5			Setup C PCam altered color		
		<i>Top-1</i>	<i>Top-20</i>	<i>All proto.</i>	<i>Top-1</i>	<i>Top-20</i>	<i>All proto.</i>	<i>Top-1</i>	<i>Top-20</i>	<i>All proto.</i>	<i>Top-1</i>	<i>Top-20</i>	<i>All proto.</i>	<i>Top-1</i>	<i>Top-20</i>	<i>All proto.</i>
Head I	✗	0.990	<b>0.993</b>	0.739	<b>0.712</b>	0.692	0.473	0.782	<b>0.852</b>	0.630	0.576	0.574	0.511	0.350	0.358	<b>0.820</b>
	✓	0.986	0.982	0.704	0.701	0.626	0.477	0.773	0.821	0.635	<b>0.579</b>	0.506	0.467	0.367	0.323	0.584
Head II-B	✗	0.972	0.984	<b>0.986</b>	0.763	0.765	0.677	0.779	0.790	0.778	0.678	0.661	0.636	0.377	0.394	0.823
	✓	0.968	0.983	0.977	0.749	0.765	0.672	0.757	<b>0.812</b>	0.777	0.673	<b>0.701</b>	0.676	0.443	0.552	<b>0.825</b>
Head III-B	✗	0.855	0.906	0.909	0.692	0.702	0.718	0.674	0.707	0.731	<b>0.687</b>	0.631	0.541	<b>0.329</b>	0.249	0.224
	✓	0.821	<b>0.948</b>	0.933	0.689	<b>0.754</b>	0.742	0.677	<b>0.780</b>	0.774	0.641	0.622	0.623	0.234	0.211	0.257

in Table III) for the PCam dataset. In Table IV, the isolation forest method achieves the best detection results on the strokes setup. Likewise, the student architectures with similarity layers before averaging (Head II-B and Head III-B) perform better in detecting strokes artifacts on the PCam dataset which is consistent with the LSUN networks. For the altered color setup, student networks with lower architectural complexity such as Head I and Head II-B architectures perform well on the altered color setup as compared to Head III-B with higher architectural complexity. The Head II-B and Head I networks using all prototypes are equally competent on the PCam altered color setting. The outliers created using the PatchCam dataset in this setting are easier to be detected as compared to the LSUN dataset due to the significant differences between the color distribution of outliers and normal PCam samples. We also observe that the ProtoDNN underperforms on the altered color setup as a majority of the outliers have a higher maximum class probability than the normal samples.

In conclusion, except for the PCam altered color setup, the use of 20 prototypes for Head-II and Head-III architectures shows better detection performances than the other prototype-based networks and comparable outlier performances to the isolation forest model. This supports our argument for unified prototype-based models with generic head architectures that are interpretable and also robust to outliers.

## VI. DISCUSSION

### A. Varying Number of Prototypes

We investigate the impact on classification performance using different number of prototypes. We use equal number of prototypes per class. We discuss only the performance for student networks with simple (Head I) and complex (Head III-B) architectures due to lack of space. Based on Figure 8, only a marginal change in performance can be seen for the simple Head I architecture on the LSUN dataset, whereas a huge decline in performance can be seen for the more complex Head III-B architecture when using a large number of prototypes (150 prototypes) due to its larger tendency to overfit. Likewise, only slight performance difference is reported for the PCam dataset with different number of prototypes. For the relatively simple PCam dataset, using small number of prototypes (20 prototypes) is sufficient and less likely to overfit as shown by the high test accuracy for both architectures. Hence, it is of a good practice to use a small number of prototypes for simple datasets and complex network architectures.

### B. Pruning of Prototypes and Relevant Neurons

Since the prototype importance weight  $\mathcal{M}$  defines the importance of the  $K$  prototypes in the network prediction, we can prune the set of prototypes with the least weight in  $\mathcal{M}$  to evaluate the impact on classification and outlier performances. We do not evaluate the LRP explanation of the pruned networks as the general architecture of the networks remains largely unchanged. We prune  $p = 30\%$  (same as  $p$  used in the iterative prototype replacement algorithm) of the prototypes and the relevant neurons, followed by finetuning of the network. Alternatively, one can set the pruning factor based on the classification performance on the validation set.

Based on Table V, we observe marginal changes in the classification performance after pruning. The pruned network with Head II-B shows a slight increase of accuracy for both datasets. The outlier detection performance of the pruned networks is reported in Table VI. The pruned networks exhibit a larger change in the outlier performance as compared to the prediction accuracy. For the LSUN dataset, the student network with Head III-B architecture consistently performs better with pruning as indicated by the significant gain in the detection performance. Since the pruning of prototypes and relevant neurons reduces the size of the network, the Head III-B network overfits less after finetuning and is more robust to outliers. We do not observe the same benefit of pruning for Head III-B on the PCam outlier setups. For the strokes setup, an evident gain in performance can be observed for Head II-B network trained on the PCam dataset. A smaller gain is seen for the Head II-B network in the altered color setup for both datasets. Thus, one may consider pruning uninformative prototypes if the network is prone to overfitting.

## VII. CONCLUSION

Various student architectures that compute prototype-based predictions were investigated for their suitability to provide example-based explanation and detect outliers. The selection of prototypical examples from the training set via the iterative prototype replacement method guaranteed meaningful explanation. The prototype similarity scores can also be used naturally to quantify the outlierness of a sample. However, the architecture with the best LRP explanation did not achieve the best outlier detection performance.

## REFERENCES

- [1] K. Simonyan, A. Vedaldi, and A. Zisserman, "Deep inside convolutional networks: Visualising image classification models and saliency maps," *arXiv preprint arXiv:1312.6034*, 2013.
- [2] M. D. Zeiler and R. Fergus, "Visualizing and understanding convolutional networks," in *European conference on computer vision*. Springer, 2014, pp. 818–833.
- [3] G. Montavon, A. Binder, S. Lapuschkin, W. Samek, and K.-R. Müller, "Layer-wise relevance propagation: an overview," in *Explainable AI: interpreting, explaining and visualizing deep learning*. Springer, 2019, pp. 193–209.
- [4] C. Cortes and V. Vapnik, "Support-vector networks," *Machine learning*, vol. 20, no. 3, pp. 273–297, 1995.
- [5] H.-M. Yang, X.-Y. Zhang, F. Yin, and C.-L. Liu, "Robust classification with convolutional prototype learning," in *Proceedings of the IEEE Conference on Computer Vision and Pattern Recognition*, 2018, pp. 3474–3482.
- [6] O. Li, H. Liu, C. Chen, and C. Rudin, "Deep learning for case-based reasoning through prototypes: A neural network that explains its predictions," *arXiv preprint arXiv:1710.04806*, 2017.
- [7] Y. Ming, P. Xu, H. Qu, and L. Ren, "Interpretable and steerable sequence learning via prototypes," in *Proceedings of the 25th ACM SIGKDD International Conference on Knowledge Discovery & Data Mining*, 2019, pp. 903–913.
- [8] C. Chen, O. Li, D. Tao, A. Barnett, C. Rudin, and J. K. Su, "This looks like that: deep learning for interpretable image recognition," in *NeurIPS*, 2019, pp. 8930–8941.
- [9] P. Hase, C. Chen, O. Li, and C. Rudin, "Interpretable image recognition with hierarchical prototypes," in *Proceedings of the AAAI Conference on Human Computation and Crowdsourcing*, vol. 7, no. 1, 2019, pp. 32–40.
- [10] D. Rymarczyk, Ł. Struski, J. Tabor, and B. Zieliński, "Protopshare: Prototype sharing for interpretable image classification and similarity discovery," *arXiv preprint arXiv:2011.14340*, 2020.
- [11] M. Nauta, R. van Bree, and C. Seifert, "Neural prototype trees for interpretable fine-grained image recognition," *arXiv preprint arXiv:2012.02046*, 2020.
- [12] K. S. Gurumoorthy, A. Dhurandhar, G. Cecchi, and C. Aggarwal, "Efficient data representation by selecting prototypes with importance weights," in *2019 IEEE International Conference on Data Mining (ICDM)*. IEEE, 2019, pp. 260–269.
- [13] B. Kim, O. Koyejo, R. Khanna *et al.*, "Examples are not enough, learn to criticize! criticism for interpretability," in *NIPS*, 2016, pp. 2280–2288.
- [14] S. O. Arik and T. Pfister, "Protoattend: Attention-based prototypical learning," *Journal of Machine Learning Research*, vol. 21, pp. 1–35, 2020.
- [15] N. S. Altman, "An introduction to kernel and nearest-neighbor non-parametric regression," *The American Statistician*, vol. 46, no. 3, pp. 175–185, 1992.
- [16] F. Angiulli and C. Pizzuti, "Fast outlier detection in high dimensional spaces," in *Principles of Data Mining and Knowledge Discovery*, T. Elomaa, H. Mannila, and H. Toivonen, Eds. Berlin, Heidelberg: Springer Berlin Heidelberg, 2002, pp. 15–27.
- [17] M. M. Breunig, H.-P. Kriegel, R. T. Ng, and J. Sander, "Lof: Identifying density-based local outliers," in *ACM SIGMOD*, 2000, p. 93–104.
- [18] L. J. Latecki, A. Lazarevic, and D. Pokrajac, "Outlier detection with kernel density functions," in *MLDM 2007*, ser. Lecture Notes in Computer Science, P. Perner, Ed., vol. 4571. Springer, 2007, pp. 61–75.
- [19] S. Kim and S. Cho, "Prototype based outlier detection," in *The 2006 IEEE International Joint Conference on Neural Network Proceedings*. IEEE, 2006, pp. 820–826.
- [20] R. Ramirez-Padron, D. Foregger, J. Manuel, M. Georgiopoulos, and B. Mederos, "Similarity kernels for nearest neighbor-based outlier detection," in *International Conference on Advances in Intelligent Data Analysis*. Berlin, Heidelberg: Springer-Verlag, 2010, p. 159–170.
- [21] X. Gu, L. Akoglu, and A. Rinaldo, "Statistical analysis of nearest neighbor methods for anomaly detection," in *NeurIPS*, H. Wallach, H. Larochelle, A. Beygelzimer, F. d'Alché-Buc, E. Fox, and R. Garnett, Eds., 2019, pp. 9233–9243. [Online]. Available: <http://papers.nips.cc/paper/9274-statistical-analysis-of-nearest-neighbor-methods-for-anomaly-detection.pdf>
- [22] D. Hendrycks and K. Gimpel, "A baseline for detecting misclassified and out-of-distribution examples in neural networks," *arXiv preprint arXiv:1610.02136*, 2016.
- [23] S. Liang, Y. Li, and R. Srikant, "Enhancing the reliability of out-of-distribution image detection in neural networks," *arXiv preprint arXiv:1706.02690*, 2017.
- [24] Y.-C. Hsu, Y. Shen, H. Jin, and Z. Kira, "Generalized odin: Detecting out-of-distribution image without learning from out-of-distribution data," in *Proceedings of the IEEE/CVF Conference on Computer Vision and Pattern Recognition*, 2020, pp. 10 951–10 960.
- [25] D. Hendrycks, M. Mazeika, and T. Dietterich, "Deep anomaly detection with outlier exposure," *arXiv preprint arXiv:1812.04606*, 2018.
- [26] F. Liu, K. Ting, and Z. Zhou, "Isolation forest," in *2008 Eighth IEEE International Conference on Data Mining*. IEEE, 2008, pp. 413–422.
- [27] D. Gong, L. Liu, V. Le, B. Saha, M. R. Mansour, S. Venkatesh, and A. v. d. Hengel, "Memorizing normality to detect anomaly: Memory-augmented deep autoencoder for unsupervised anomaly detection," in *Proceedings of the IEEE International Conference on Computer Vision*, 2019, pp. 1705–1714.
- [28] O. Eberle, J. Büttner, F. Kräutli, K.-R. Müller, M. Valleriani, and G. Montavon, "Building and interpreting deep similarity models," *arXiv preprint arXiv:2003.05431*, 2020.
- [29] F. Yu, A. Seff, Y. Zhang, S. Song, T. Funkhouser, and J. Xiao, "Lsun: Construction of a large-scale image dataset using deep learning with humans in the loop," *arXiv preprint arXiv:1506.03365*, 2015.
- [30] B. E. Bejnordi, M. Veta, P. J. Van Diest, B. Van Ginneken, N. Karssemeijer, G. Litjens, J. A. Van Der Laak, M. Hermesen, Q. F. Manson, M. Balkenhol *et al.*, "Diagnostic assessment of deep learning algorithms for detection of lymph node metastases in women with breast cancer," *Jama*, vol. 318, no. 22, pp. 2199–2210, 2017.
- [31] B. S. Veeling, J. Linmans, J. Winkens, T. Cohen, and M. Welling, "Rotation equivariant cnns for digital pathology," in *MICCAI*. Springer, 2018, pp. 210–218.
- [32] M.-E. Nilsback and A. Zisserman, "Automated flower classification over a large number of classes," in *2008 Sixth Indian Conference on Computer Vision, Graphics & Image Processing*. IEEE, 2008, pp. 722–729.
- [33] P. Chong, L. Ruff, M. Kloft, and A. Binder, "Simple and effective prevention of mode collapse in deep one-class classification," in *IJCNN 2020*, 2020, pp. 1–9.
- [34] K. He, X. Zhang, S. Ren, and J. Sun, "Deep residual learning for image recognition," in *Proceedings of the IEEE conference on computer vision and pattern recognition*, 2016, pp. 770–778.
- [35] A. Paszke, S. Gross, S. Chintala, G. Chanan, E. Yang, Z. DeVito, Z. Lin, A. Desmaison, L. Antiga, and A. Lerer, "Automatic differentiation in pytorch," 2017.
- [36] A. Vedaldi and A. Zisserman, "Efficient additive kernels via explicit feature maps," *IEEE transactions on pattern analysis and machine intelligence*, vol. 34, no. 3, pp. 480–492, 2012.
- [37] W. Samek, A. Binder, G. Montavon, S. Lapuschkin, and K.-R. Müller, "Evaluating the visualization of what a deep neural network has learned," *IEEE TNNLS*, vol. 28, no. 11, pp. 2660–2673, 2016.

**Penny Chong** is a Ph.D. student at the Singapore University of Technology and Design (SUTD), under the supervision of Alexander Binder and Ngai-Man Cheung. She received a B.Sc. (Hons) in Applied Mathematics with Computing from Universiti Tunku Abdul Rahman (UTAR), Malaysia in 2016. Her research interests include machine learning, explainable AI and its applications.

**Ngai-Man Cheung** is an associate professor at the Singapore University of Technology and Design (SUTD). He received his Ph.D. degree in Electrical Engineering from University of Southern California (USC), Los Angeles, CA, in 2008. His research interests include image and signal processing, computer vision and AI.

**Yuval Elovici** is the director of the Telekom Innovation Laboratories at Ben-Gurion University of the Negev (BGU), head of BGU Cyber Security Research Center and a professor in the Department of Software and Information Systems Engineering at BGU. He holds a Ph.D. in Information Systems from Tel-Aviv University. His primary research interests are computer and network security, cyber security, web intelligence, information warfare, social network analysis, and machine learning. He is the co-founder of the start-up Morphisec.

**Alexander Binder** is an associate professor at the University of Oslo (UiO). He received a Dr.rer.nat. in Computer Science from Technische Universität Berlin in 2013. His research interests include explainable deep learning and medical imaging.